crystals

MDPI

Supplementary Materials

Novel Cerium Bisphosphinate Coordination Polymer and Unconventional Metal-Organic Framework

Jan Rohlíček [1], Daniel Bůžek [2], Petr Brázda [1], Libor Kobera [3], Jan Hynek [2], Jiří Brus [3], Kamil Lang [2] and Jan Demel [2,*]

[1] Institute of Physics of the Czech Academy of Sciences, 18221 Prague, Czech Republic
[2] Institute of Inorganic Chemistry of the Czech Academy of Sciences, Husinec-Řež 1001, 250 68 Řež, Czech Republic;
[3] Institute of Macromolecular Chemistry of the Czech Academy of Sciences, Heyrovského nám. 2, 162 06, Prague 6, Czech Republic
* Correspondence: demel@iic.cas.cz

Received: date; Accepted: date; Published: date

Table of content

Table S2. Crystallographic details of ICR-9.

Formula	$C_{24}H_{30}Ce_2O_{12}P_6$
Crystal system	Hexagonal
Space group	$P6_3/m$
Radiation	electrons, 120 kV, 0.0335 Å
a (Å)	17.4(1)
c (Å)	40.7(5)
V (Å^3)	10661
Z	12
Frames /irradiation time (s)	120 /0.4
Instrument	Philips CM120, SIS Veleta 14bit CCD
Processing software	PETS, Jana2006, Dyngo
Measured reflns.	3349
Observed reflns. (I>3σ(I))	1704
Number of parameters /number of restraints	150/ 89
Hydrogen refinement	geometrically restrained
R(obs), wR(all)	0.3317, 0.3524

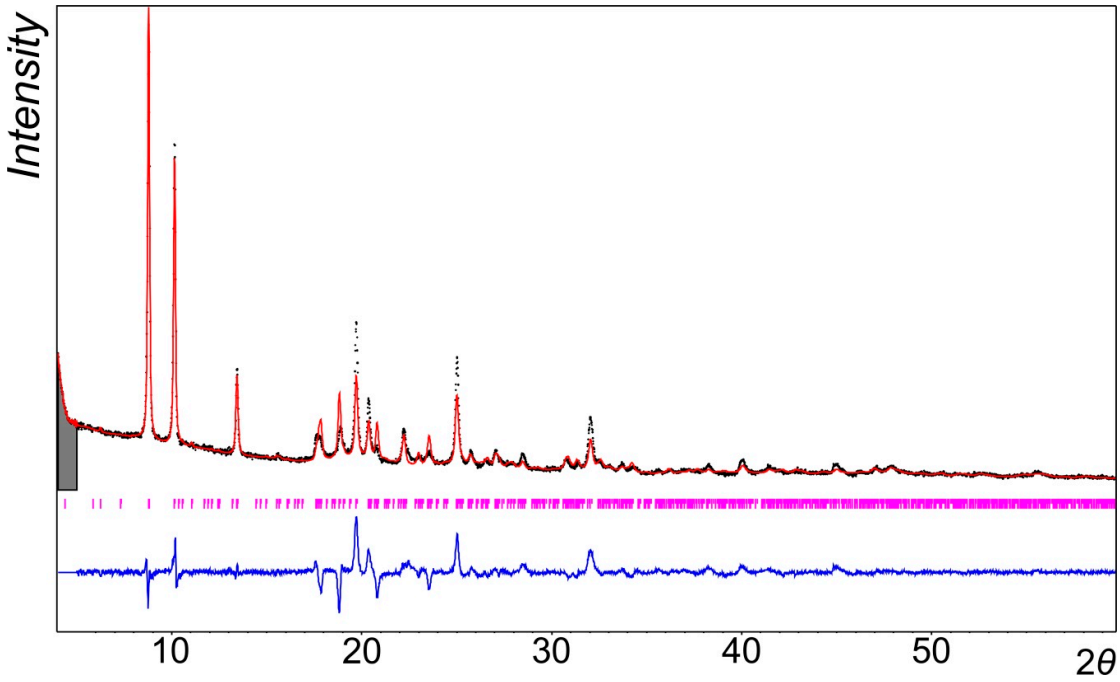

Figure S1. Rietveld fit of ICR-9Cryst. Black dots represent measured data, red curve is a calculated profile, blue line is a difference curve and magenta vertical bars are Bragg's positions of the *hkl* reflections.

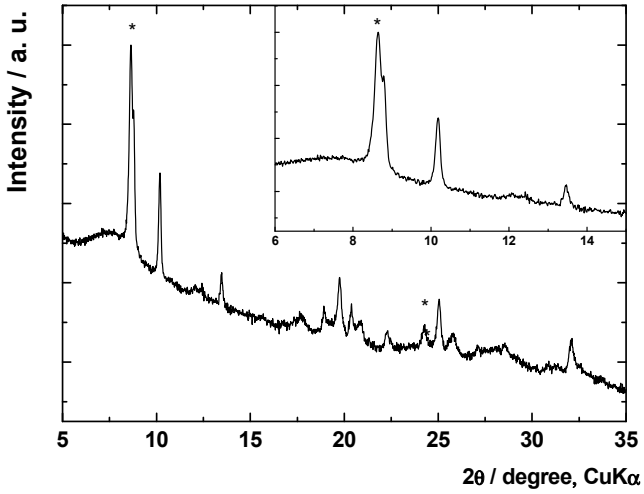

Figure S2. Powder XRD pattern of the sample prepared by the defective procedure with a reaction time of 3 h. The unknown phase is marked with asterisk.

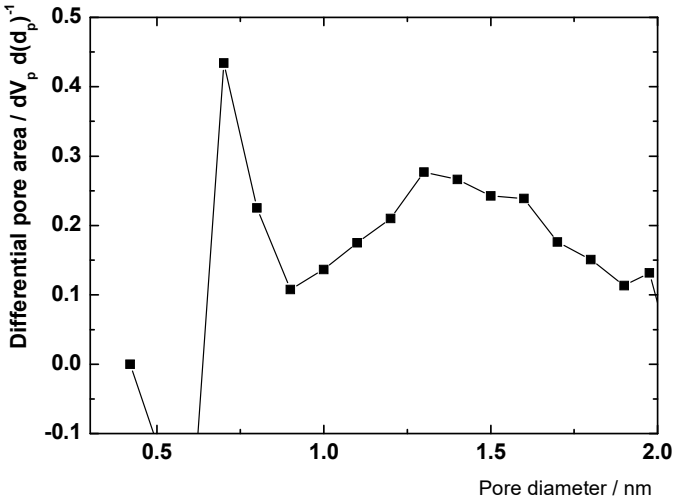

Figure S3. Pore size distribution of ICR-9A calculated by the MP plot.

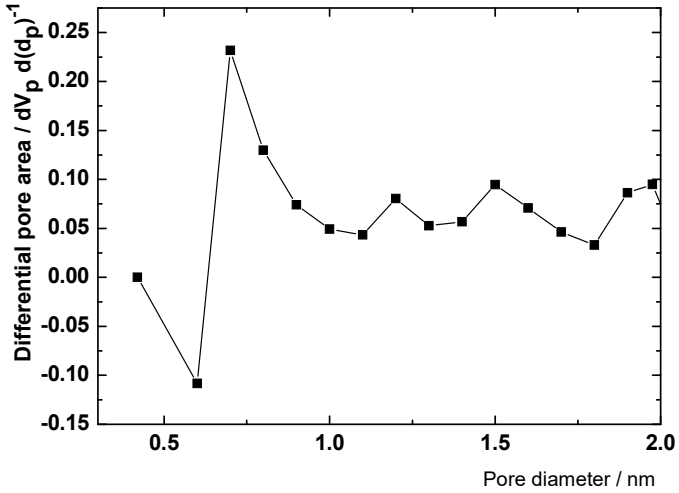

Figure S4. Pore size distribution of ICR-9B calculated by the MP plot.

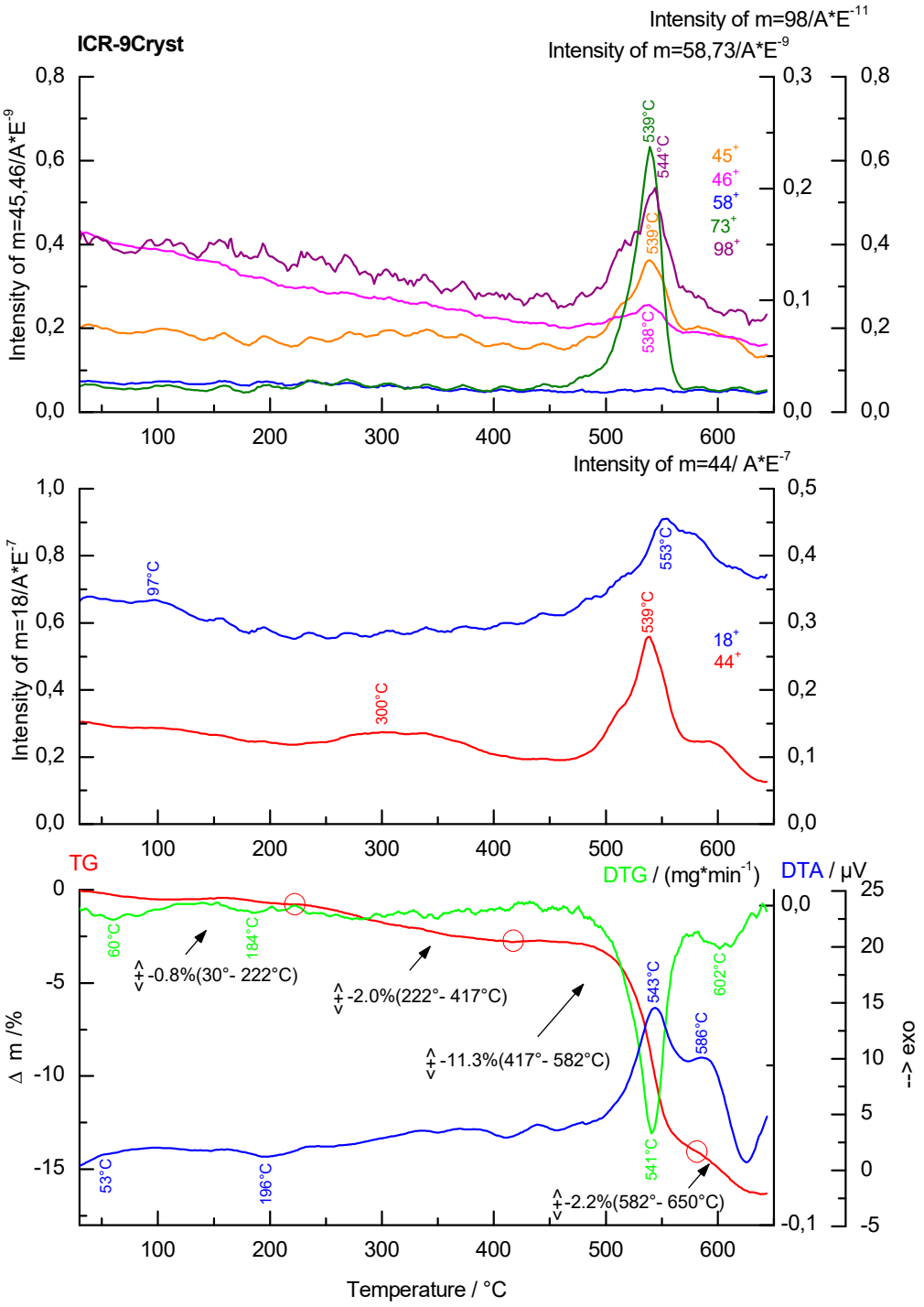

Figure S5. DTA/TGA curves (bottom) and the evolution of gases (top) for ICR-9Cryst. Mass peaks: 18^+ = H_2O; 44^+ = CO_2; 45^+ = dimethylamine; 46^+ = formic acid; 58^+ = acetone; 98^+ = H_3PO_4. Above 500°C, an unknown product evolves with a mass peak of 73^+, this is a product of combustion of ICR-9 and not DMF because DMF was detected neither by elemental analysis nor ssNMR. The measurement was performed in synthetic air from room temperature to 650 °C with a heating rate of 10 °C min^{-1}.

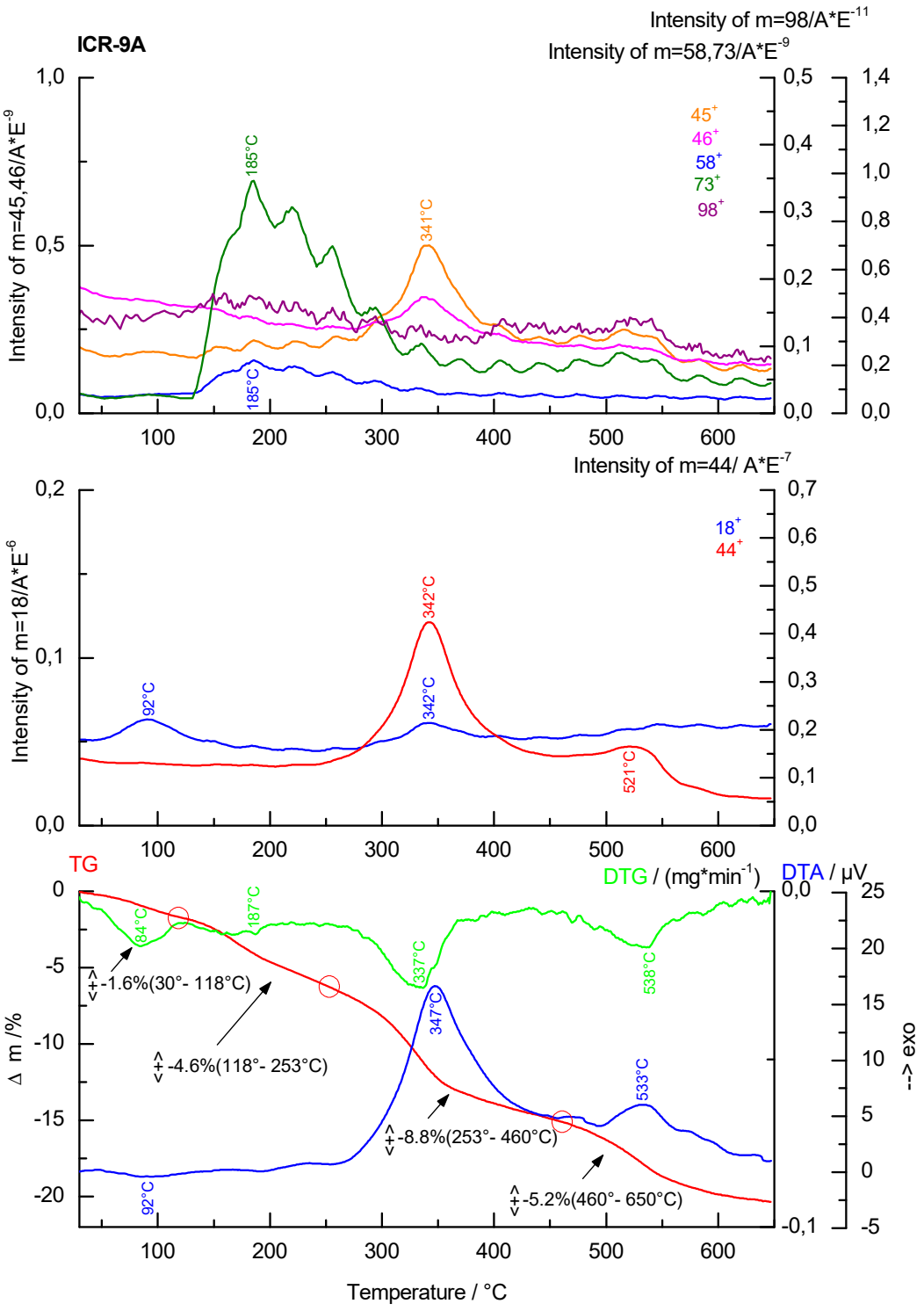

Figure S6. DTA/TGA curves (bottom) and the evolution of gases (top) for ICR-9A. Mass peaks: 18^+ = H_2O; 44^+ = CO_2; 45^+ = dimethylamine; 46^+ = formic acid; 58^+ = acetone; 73^+ = DMF; 98^+ = H_3PO_4; the presence of formic acid and dimethylamine is connected with DMF thermal decomposition. The measurement was performed in synthetic air from room temperature to 650 °C with a heating rate of 10 °C min^{-1}.

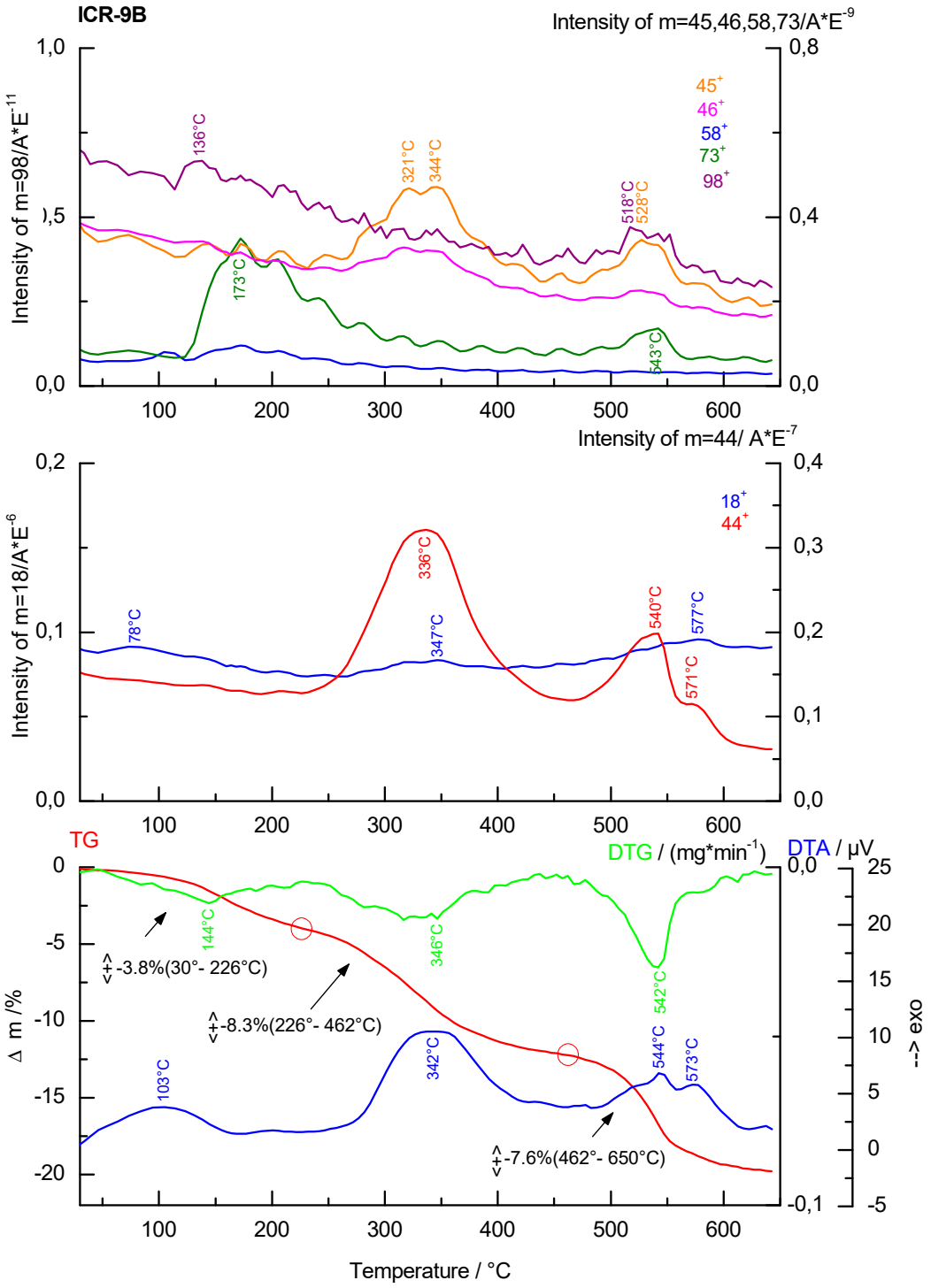

Figure S7. DTA/TGA curves (bottom) and the evolution of gases (top) for ICR-9B. Mass peaks: 18^+ = H_2O; 44^+ = CO_2; 45^+ = dimethylamine; 46^+ = formic acid; 58^+ = acetone; 73^+ = DMF; 98^+ = H_3PO_4; the presence of formic acid and dimethylamine is connected with DMF thermal decomposition. The measurement was performed in synthetic air from room temperature to 650 °C with a heating rate of 10 °C min^{-1}.

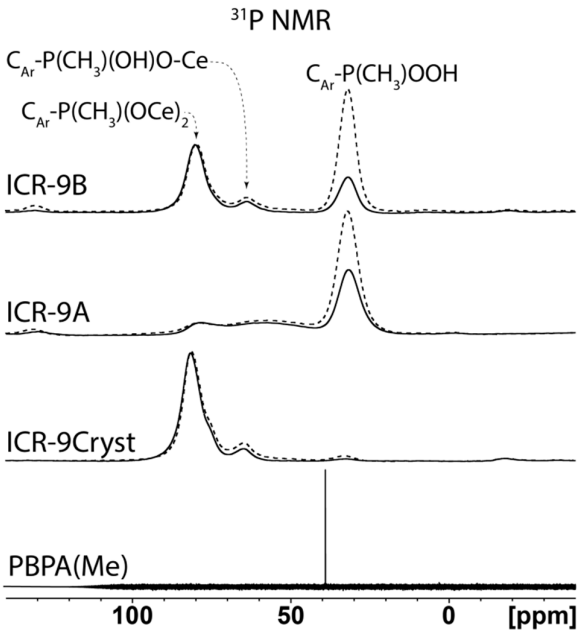

Figure S8. Assignment of ^{31}P peaks in the ssNMR spectra: ^{31}P NMR spectrum of H_2PBP(Me) measured in liquid state, ^{31}P MAS (solid line) and CP/MAS (dashed line) NMR spectra of prepared ICR-9 systems.

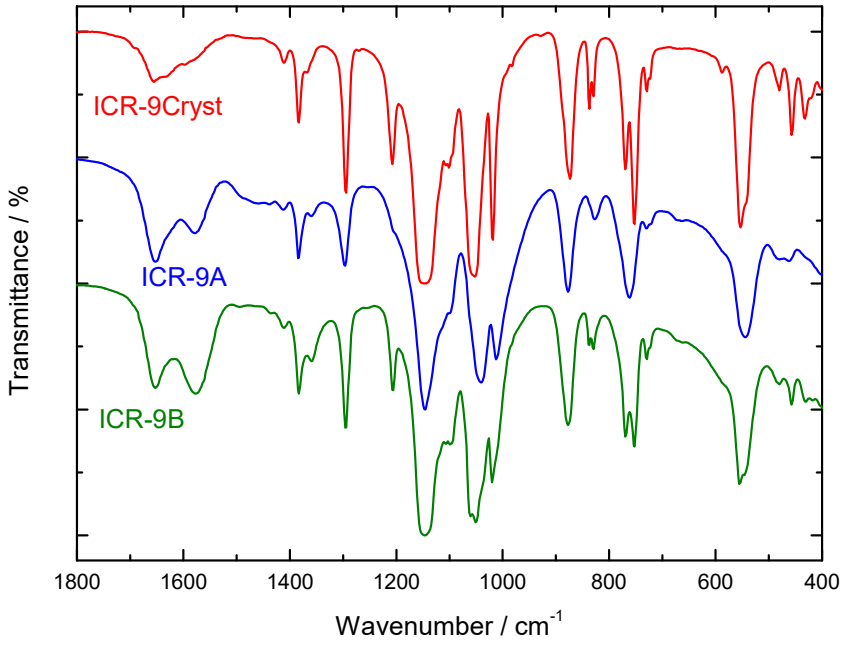

Figure S9. FTIR spectra of the ICR-9Cryst (red), ICR-9A (blue), and ICR-9B (green). The spectra are normalized and vertically shifted to avoid overlaps. The absorptions of ICR-9Cryst are better resolved than in the cases of ICR-9A and ICR-9B. It reflects better ordering of the crystalline ICR-9 phase in comparison with UMOF.